Advances in Computational Design, *Vol. 5, No. 4 (2020) 397-416*
DOI: https://doi.org/10.12989/acd.2020.5.4.397

Buckling analysis of noncontinuous linear and quadratic axially graded Euler beam subjected to axial span-load in the presence of shear layer

Abbas Heydari*

Department of civil engineering, Faculty of Razi, Ardabil branch, Technical and Vocational University (TVU), Ardabil, Iran

(Received November 12, 2019, Revised February 11, 2020, Accepted February 12, 2020)

Abstract. Functionally graded material (FGM) illustrates a novel class of composites that consists of a graded pattern of material composition. FGM is engineered to have a continuously varying spatial composition profile. Current work focused on buckling analysis of beam made of stepwise linear and quadratic graded material in axial direction subjected to axial span-load with piecewise function and rested on shear layer based on classical beam theory. The various boundary and natural conditions including simply supported (S-S), pinned – clamped (P-C), axial hinge – pinned (AH-P), axial hinge – clamped (AH-C), pinned – shear hinge (P-SHH), pinned – shear force released (P-SHR), axial hinge – shear force released (AH-SHR) and axial hinge – shear hinge (AH-SHH) are considered. To the best of the author's knowledge, buckling behavior of this kind of Euler-Bernoulli beams has not been studied yet. The equilibrium differential equation is derived by minimizing total potential energy via variational calculus and solved analytically. The boundary conditions, natural conditions and deformation continuity at concentrated load insertion point are expressed in matrix form and nontrivial solution is employed to calculate first buckling loads and corresponding mode shapes. By increasing truncation order, the relative error reduction and convergence of solution are observed. Fast convergence and good compatibility with various conditions are advantages of the proposed method. A MATLAB code is provided in appendix to employ the numerical procedure based on proposed method.

Keywords: buckling; stepwise axially graded beam; linear and quadratic material gradation; piecewise load function; shear layer

1. Introduction

The conventional engineering materials and composites are not able to meet the many required properties of applications in various fields of science including power generation, aerospace, automotive, microelectronics, structural and bioengineering. These applications require mutually exclusive properties to withstand against chemical aggressive environment and thermo-mechanical stresses. The property distribution is evadable in many tools that must have multiple functions. For example, gears must be tough enough inside to resist the fracture but must also be hard on the outside to avoid wear. The turbine blade must be tough to bear loading, but it must also have a high melting point to withstand high temperatures on the outer surface. Functionally Graded

*Corresponding author, Technical Assistant Professor, E-mail: a_heydari@alum.sharif.edu, a_heydari@tabrizu.ac.ir

Material (FGM) was proposed for composites and polymeric materials to imitate the structure and behavior of natural materials like bones, teeth and Bamboo trees. FGM exhibits many advantages compared to conventional alloys and composite materials due to property distribution (El-Galy *et al*. 2019).

The analyses of FG beams (Heydari 2011, 2018a, Heydari and Jalali 2017, Kang *et al*. 2019, Li *et al*. 2018, Li *et al*. 2017, She *et al*. 2017, She *et al*. 2017c), FG tubes (She *et al*. 2017a), FG plates (Heydari 2018c, Lal *et al*. 2019a, 2019b, 2019c, Magnucka-Blandzi *et al*. 2018, Ting *et al*. 2019, Yang *et al*. 2018), FG vessel and sphere (Heydari 2009, 2015, 2019), FG microbeam (Fang *et al*. 2018), FG nanobeam (She *et al*. 2019, She *et al*. 2018, She *et al*. 2019), FG nanotube (She *et al*. 2018a, 2018b, 2018c, She *et al*. 2017) and FG shell (She 2017b) are conducted. A review on stability, buckling and free vibration analyses of FGM is performed (Kang *et al*. 2019). The various methods are used in engineering problems (Ismail *et al*. 2018, Toghroli *et al*. 2018). The analytical solution is used to study buckling of FG plate (Heydari 2013) and investigate asymmetric transient responses of annular/circular viscoelastic plate (Alavi and Eipakchi 2020). Exact vibration and buckling analyses of arbitrary gradation of nano-higher order rectangular beam is done (Heydari 2018b). The buckling analysis of tapered FG circular plate rested on Pasternak medium based on HSDT is done and data in literature are improved by introducing a new displacement field (Heydari *et al*. 2017). Elastoplastic thermal buckling characteristics of ceramic-metal FGM beam under non-uniform temperature rise in transverse direction are studied via symplectic method in Hamiltonian system (Zhang *et al*. 2019). Inhomogeneity and porosity effects on the buckling and vibration of double-FGM nanoplates via a quasi-3D refined theory are investigated (Sobhy and Zenkour 2019). Thermo-mechanical buckling analysis of functionally graded graphene nanoplatelets reinforced micro plate based on modified strain gradient theory is done (Arefi *et al*. 2019). Vibration control analysis of a rotating flexible FGM beam with an attached lumped mass in temperature field is carried out (Liang Li *et al*. 2019). Material properties variations and negative Poisson's ratio effects on thermal post-buckling of sandwich beams with FG honeycomb core are examined (Li. *et al*. 2019). The unified model of buckling and free vibration of linearly tapered axially functionally graded columns with arbitrary material gradation is proposed (Lee and Lee 2019). Exact buckling analysis of cantilever columns with exponential material gradation in axial direction rested on rotational spring hinge is performed and the approximate explicit expression for buckling loads of heterogeneous columns is proposed (Xiao and Li 2019). The weak form quadrature plate element with stiffeners located anywhere other than along a nodal line is formulated to calculate simultaneous overall and local buckling of stiffened panels (Deng *et al*. 2019). A novel theory for the buckling analysis of circular arches including shear deformation is developed. The buckling of arches for uniform axial forces and incorporating the effect of pre-buckling deformations and all internal forces are performed and validated by finite element method (FEM). The buckling of arches with shear deformation is then viewed as an interactive buckling between flexural and shear buckling (Chengyi *et al*. 2020). Based on trigonometric and polynomial shape functions, the different equivalent single layer and layer wise theories are employed to calculate maximum tensile and compressive strains under buckling condition via Rayleigh-Ritz approximation technique (Kharghani *et al*. 2020). Buckling analyses of Levy-type plates restrained by point-supports are studied (Hu *et al*. 2019). The static, stability and Free vibration analyses of tapered bidirectional functionally graded thin-walled non-prismatic Euler beams of generic open/closed sections are studied (Rajasekaran and Khaniki 2019). A new semi-analytical method for local buckling analysis of moderately thick-walled laminated doubly-symmetric I-beams subjected to the uniaxial compression load is proposed. In contrast to the

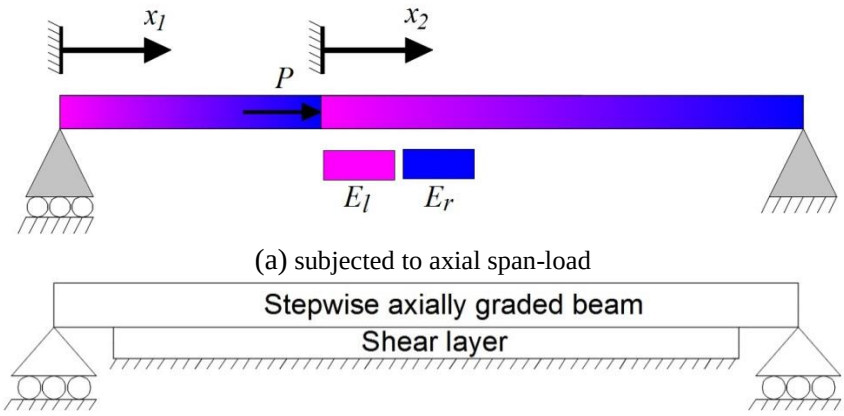

(a) subjected to axial span-load

(b) rested on shear layer

Fig. 1 Stepwise axially graded beam

frequently used approach of discrete plate analysis for local beam buckling calculations, the series expansions for all buckling freedom degrees and a subsequent assembly are used to consider the interaction between flanges and webs by employing sufficient continuity conditions at adjacent segments of the cross-sections intersect (Mittelstedt and Mittelstedt 2019). Small deformation theory is applied and differences in line-contact between springy-wall-beam and rigid-wall-beam are discussed in deformation and displacement and force controls vibration of a buckled beam constrained by springy walls. The results of Galerkin approximation and analytical method are compared (Chen and Wen 2019). The buckling governing equation of Timoshenko type beam with sharp and smooth beam edges rested on elastic half-plane is solved via Chebyshev polynomials and Galerkin method. The effect of main parameters variations on buckling loads and corresponding mode shapes are investigated (Falope *et al*. 2019). Elastoplastic nonlinear behavior of planar steel gabled frame is investigated (Heyrani *et al*. 2019). Buckling assessment of dented truncated cones under external pressure (Ghanbari *et al*. 2016) and seismic response analysis of mega-scale buckling-restrained bracing systems in tall buildings (Gholipour and Mazloom 2018) are carried out.

Present work aims to investigate the effects of linear and quadratic material gradation in the axial direction as well as piecewise compressive axial span-load function on buckling behavior of Euler-Bernoulli beam rested on shear layer. The various boundary and natural conditions including simply supported (S-S), pinned – clamped (P-C), axial hinge – pinned (AH-P), axial hinge – clamped (AH-C), pinned – shear hinge (P-SHH), pinned – shear force released (P-SHR), axial hinge – shear force released (AH-SHR) and axial hinge – shear hinge (AH-SHH) are considered. The same results are obtained based on stepwise solution and nontrivial solution; consequently the validity of the results is proved. First buckling loads and corresponding mode shapes are calculated and presented. In the case of quadratic material gradation in the axial direction, the approximated series is used by considering first finite terms of truncated series instead of infinite series of bases. The convergence of the solution as well as relative error reduction is observed by increasing terms. The roots of characteristic equation are obtained by employing Newton iteration method. In stepwise solution method, calculating unknown coefficients is requisite; therefore more computational efforts are required. Fast convergence and good compatibility with various

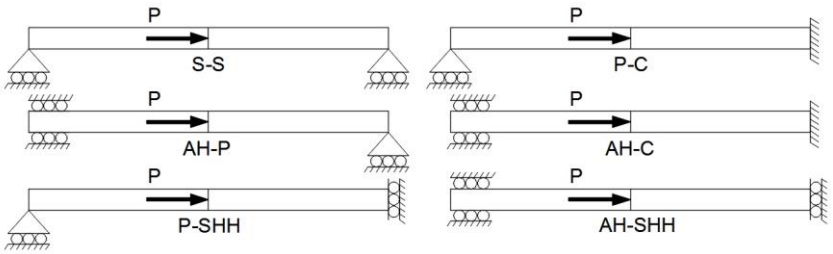

Fig. 2 Axially graded beam with various boundary conditions

conditions are benefits of the proposed method based on nontrivial solution. The matrix operations are employed to calculate shape modes of corresponding buckling loads. The buckling analysis of beam with stepwise linear and quadratic axial material gradation subjected to axial span-load and rested on shear layer based on the proposed method is performed by writing a MATLAB code.

2. Governing equations

The thin beam is composed of two distinct parts with the similar material gradation pattern in the axial direction. The mathematical function of the elasticity modulus in the global coordinate system is discontinues at junction of the parts; hence beam has a stepwise axial material gradation. Fig. 1 illustrates continues variation of the modulus of elasticity in the axial direction in each part of the beam. The elasticity modulus at left end, E_l, is turned into the elasticity modulus at right end, E_r, continuously. In the pre-buckling stage, the left part of the beam is assumed to be stress-free; as a result, the mathematical function of the axial loading is a piecewise function.

The stepwise axially graded Euler-Bernoulli beams subjected to axial span-load with various boundary conditions are demonstrated in Fig. 2.

The elasticity modulus variation of linear and quadratic axially graded Euler-Bernoulli beam is modeled by gradation functions in Eq. (1).

$$E(x_i) = E_l + E_s\left(\frac{x_i}{l_i}\right)^n \qquad i,n \in \{1,2\} \tag{1}$$

in which l_i is length of the part i. The parameter n is material index. The difference of elasticity modulus at left end, E_l and right end, E_r is $E_s = E_r - E_l$. The parameter E takes positive values, therefore in the case of negative gradation ($E_s < 0$), the inequality $|E_s| < E_l$ must be satisfied. The total potential energy can be written as

$$\Pi = U + \Omega \tag{2}$$

The stored strain energy and path-dependent work caused by non-conservative force are shown by U and Ω, respectively.The total potential energy of buckled linear and quadratic axially graded Euler-Bernoulli beam rested on shear layer is

$$\Pi = \frac{1}{2}\int_0^L IE(x)\left(y''(x)\right)^2 - Gy''(x)y(x)dx - \frac{1}{2}P\int_0^L \delta l(x) \tag{3}$$

where the parameters I, y, G, P and $\delta l(x)$ denote moment of inertia, deflection, shear modulus of shear layer, concentrated axial compression applied to the junction of the beam parts and change of the beam element length caused by buckling at the position x, respectively. It is noteworthy that the parameter $\delta l(x)$ takes positive sign when decrease in length occurs. The total change of the beam length subjected to compressive load can be calculated as follows

$$\Delta L = \int_0^L \left(\sqrt{1 + \left(y'(x)\right)^2} - 1 \right) dx \tag{4}$$

The integrand in second term of Eq. (3) is replaced by truncated Taylor series expansion with truncation order of three. Eq. (3) is rewritten as follows

$$\Pi = \frac{1}{2} \int_0^L IE(x)\left(y''(x)\right)^2 - Gy''(x)y(x)dx - \frac{1}{2} P \int_0^L \left(y'(x)\right)^2 dx \tag{5}$$

The total potential energy must be minimized to calculate governing equilibrium equation. To this purpose, instead of y, the auxiliary path, $\tilde{y}$, is used.

$$\tilde{y}(x) = y(x) + \eta(x)\xi \tag{6}$$

The smooth function $\eta(x)$ can be differentiated at least twice. Moreover, $\eta(x)$ and its derivatives are vanished at both ends of the beam. The parameter ξ is a real variable. The derivative of Π with respect to ξ is calculated to minimize total potential energy.

$$\lim_{\xi \to 0} \frac{\partial}{\partial \xi} \left(\int_0^L EI(\tilde{y}'')^2 - G\tilde{y}''\tilde{y}dx - P \int_0^L (\tilde{y}')^2 dx \right) = 0 \tag{7}$$

The chain rule is employed as follows ($I = Cte$):

$$\frac{1}{2} \lim_{\xi \to 0} \left(\int_0^L EI \frac{\partial}{\partial \tilde{y}''} (\tilde{y}'')^2 \frac{\partial \tilde{y}''}{\partial \xi} - G \left(\frac{\partial \tilde{y}''}{\partial \xi} \tilde{y} + \frac{\partial \tilde{y}}{\partial \xi} \tilde{y}'' \right) dx - P \int_0^L \frac{\partial}{\partial \tilde{y}'} (\tilde{y}')^2 \frac{\partial \tilde{y}'}{\partial \xi} dx \right) = 0 \tag{8}$$

Eq. (8) is simplified as follows

$$\int_0^L EIy''\eta'' - \frac{1}{2} G(\eta''y + \eta y'')dx - P \int_0^L y'\eta' dx = 0 \tag{9}$$

According to integration by parts rule, one can write

$$EI\,(y''\eta') - P(y'\eta) - \frac{1}{2} G\eta' y \Big]_{x=0}^{x=L} - \int_0^L \eta' I(Ey'')' + \frac{1}{2} G\left(\eta y'' - \eta' y'\right)dx + P \int_0^L y''\eta dx = 0 \tag{10}$$

The integration by parts rule is employed again.

$$\left(\frac{1}{2} Gy' - I(Ey'')' \right) \eta \Big]_{x=0}^{x=L} + \int_0^L (I(Ey'')'' + (P - G)y'')\eta dx = 0 \tag{11}$$

Eq. (11), shows that the integrand must be set equal to zero. For $n = 1$, one has

$$\left((E_0 L + E_s x) y^{(4)} + 2E_s y''' \right) I + (P - G)Ly'' = 0 \tag{12}$$

For $n = 2$, it holds

$$\left((E_0L^2 + E_sx^2)y^{(4)} + 4E_sxy''' + 2E_sy''\right)I + (P - G)L^2y'' = 0 \tag{13}$$

3. Deflection function

The solution of the governing differential equations is

$$y(x_2) = c_1y_1(x_2) + c_2y_2(x_2) + y_r(x_2) \tag{14}$$

The function $y_r(x_2)$ denotes rigid body motion.

$$y_r(x_2) = c_3x_2 + c_4 \tag{15}$$

For $n = 1$, the bases y_1 and y_2 are

$$y_1 = J_1\left(2\sqrt{\frac{(E_ll_2^2 + E_sx_2l_2)(P - G)}{E_s^2I}}\right)\sqrt{\left(E_l + E_s\frac{x_2}{l_2}\right)I} \tag{16}$$

$$y_2 = Y_1\left(2\sqrt{\frac{(E_ll_2^2 + E_sx_2l_2)(P - G)}{E_s^2I}}\right)\sqrt{\left(E_l + E_s\frac{x_2}{l_2}\right)I} \tag{17}$$

where J and Y are Bessel functions of the first and second kinds, respectively. The subscript one denotes the order of the Bessel functions. For $n = 2$, the bases y_1 and y_2 are

$$y_1 = \sqrt{\pi}I\left(E_s\left({}^{x_2}/_{l_2}\right)^2 + E_l\right)\sum_{n=0}^{\infty}\frac{\Gamma(\mu_1 + n)\Gamma(\mu_2 + n)X^n}{\Gamma(\mu_1)\Gamma(\mu_2)\Gamma(0.5 + n)n!} \tag{18}$$

$$y_2 = \sqrt{\pi}Ix\left(E_s\left({}^{x_2}/_{l_2}\right)^2 + E_l\right)\sum_{n=0}^{\infty}\frac{\Gamma(\mu_3 + n)\Gamma(\mu_4 + n)X^n}{\Gamma(\mu_3)\Gamma(\mu_4)\Gamma(1.5 + n)n!} \tag{19}$$

The gamma function is defined as follows

$$\Gamma(k) = \int_0^{\infty} x^{k-1}e^{-x}\ dx \tag{20}$$

The dimensionless parameters μ_1 to μ_4 are

$$\mu_1 = \frac{3}{4} - \frac{1}{2}\sqrt{\frac{1}{4} - \frac{(P - G)l_2^2}{(E_r - E_l)I}} \tag{21}$$

$$\mu_2 = \frac{3}{4} + \frac{1}{2}\sqrt{\frac{1}{4} - \frac{(P - G)l_2^2}{(E_r - E_l)I}} \tag{22}$$

$$\mu_3 = \frac{5}{4} - \frac{1}{2}\sqrt{\frac{1}{4} - \frac{(P-G)l_2^2}{(E_r - E_l)I}} \tag{23}$$

$$\mu_4 = \frac{5}{4} + \frac{1}{2}\sqrt{\frac{1}{4} - \frac{(P-G)l_2^2}{(E_r - E_l)I}} \tag{24}$$

The dimensionless function X is

$$X = -\frac{Es}{E_l}\left(\frac{x_2}{l_2}\right)^2 \tag{25}$$

By approaching P to zero, the deflection of axially graded beam in the absence of axial compression will be obtained.

$$\bar{y}(x) = c_5\bar{y}_1(x_1) + c_6\bar{y}_2(x_1) + \bar{y}_r(x_1) \tag{26}$$

in which

$$\bar{y}_r(x_1) = c_7x_1 + c_8 \tag{27}$$

For $n = 1$, Eq. (28) and Eq. (29) are calculated.

$$\bar{y}_r(x_1) = c_7x_1 + c_8 \tag{28}$$

$$\bar{y}_2 = \left(x_1 + \frac{E_l}{E_s}l_1\right)\ln\left(x_1 + \frac{E_l}{E_s}l_1\right) \tag{29}$$

For $n = 2$, Eq. (30) and Eq. (31) are obtained.

$$\bar{y}_1 = 2x_1\tan^{-1}\left(\frac{x_1E_s}{l_1\sqrt{E_lE_s}}\right)E_s - l_1\sqrt{E_lE_s}\ln\left(\frac{E_ll_1^2 + E_sx_1^2}{E_ll_1^2}\right) \tag{30}$$

$$\bar{y}_2 = 2E_ll_1\tan^{-1}\left(\frac{x_1E_s}{l_1\sqrt{E_lE_s}}\right) + x_1\ln(E_ll_1^2 + E_sx_1^2)\sqrt{E_lE_s} \tag{31}$$

4. Characteristic equation

Two approaches are used to validate calculated numerical results. The first method for obtaining characteristic equation is based on stepwise or direct solution of boundary and natural equations, while the second method is based on nontrivial solution.

4.1 First method: Stepwise solution

In this section the characteristic equation of pinned-pinned beam is calculated. The similar procedure can be employed to calculate buckling loads and corresponding mode shapes of beam

with other boundary conditions. The boundary conditions at left part of the beam ($\bar{y}(0) = \bar{y}''(0) = 0$) are considered and some unknown coefficients in Eq. (26) are calculated ($c_5 = \alpha c_8, c_6 = \beta c_8$).

$$\alpha = \frac{\bar{y}_2''|_{x_1=0}}{\bar{y}_2(0)\bar{y}_1''|_{x_1=0} - \bar{y}_2''|_{x_1=0}\bar{y}_1(0)} \tag{32}$$

$$\beta = -\frac{\bar{y}_1''|_{x_1=0}}{\bar{y}_2(0)\bar{y}_1''|_{x_1=0} - \bar{y}_2''|_{x_1=0}\bar{y}_1(0)} \tag{33}$$

The same calculations ($y(l_2) = y''(l_2) = 0$) are conducted for right part of the beam ($c_1 = \gamma(l_2c_3 + c_4), c_2 = \delta(l_2c_3 + c_4)$).

$$\gamma = \frac{y_2''|_{x_2=l_2}}{y_2(l_2)y_1''|_{x_2=l_2} - y_2''|_{x_2=l_2}y_1(l_2)} \tag{34}$$

$$\delta = -\frac{y_1''|_{x_2=l_2}}{y_2(l_2)y_1''|_{x_2=l_2} - y_2''|_{x_2=l_2}y_1(l_2)} \tag{35}$$

The deformation continuity at junction of the two parts is considered ($\bar{y}(l_1) = y(0), \bar{y}'(l_1) = y'(0)$) and the constants c_7 and c_8 are calculated in terms of the constants c_3 and c_4.

$$c_7 = \varepsilon_1 c_3 + \varepsilon_2 c_4 \tag{36}$$

$$c_8 = \varepsilon_3 c_3 + \varepsilon_4 c_4 \tag{37}$$

The parameter d in Eq. (36) and Eq. (37) denotes denominator, which is a numeral constant. The unknown parameters in Eq. (36) and Eq. (37) are defined as follows

$$\varepsilon_1 = \frac{\lambda + \xi l_2}{d} \tag{38}$$

$$\varepsilon_2 = \frac{\xi - \eta}{d} \tag{39}$$

$$\varepsilon_3 = \frac{\psi l_2 - l_1}{d} \tag{40}$$

$$\varepsilon_4 = \frac{1 + \psi}{d} \tag{41}$$

$$\zeta = \gamma y_1'(0) + \delta y_2'(0) \tag{42}$$

$$\eta = \alpha y_1'(l_1) + \beta y_2'(l_1) \tag{43}$$

$$\lambda = \alpha y_1(l_1) + \beta y_2(l_1) + 1 \tag{44}$$

$$\xi = \zeta \ \lambda - \eta\big(\gamma y_1(0) + \delta y_2(0)\big) \tag{45}$$

$$\psi = \gamma\big(y_1(0) - l_1 y_1'(0)\big) + \delta\big(y_2(0) - l_1 y_2'(0)\big) \tag{46}$$

$$d = \alpha\big(y_1(l_1) - l_1 y_1'(l_1)\big) + \beta\big(y_2(l_1) - l_1 y_2'(l_1)\big) + 1 \tag{47}$$

The relation between constants c_3 and c_4 can be obtained by satisfying equilibrium of the internal bending moments at axial load insertion point.

$$(E_s + E_l)\frac{d^2}{dx_1^2}\bar{y}(x_1)\bigg|_{x_1=l_1} - E_l\frac{d^2}{dx_2^2}y(x_2)\bigg|_{x_2=0} = 0 \tag{48}$$

The relation between c_3 and c_4 is $c_3 = \Theta c_4$.

$$\Theta = \frac{\epsilon_4\chi \ - \varsigma}{\varsigma l_2 - \epsilon_3\chi} \tag{49}$$

$$\chi = \big(\alpha y_1''(l_1) + \beta y_2''(l_1)\big)(E_l + E_r) \tag{50}$$

$$\varsigma = \big(\gamma y_1''(0) + \delta y_2''(0)\big)E_l \tag{51}$$

The deflection functions of two parts are recalculated in terms of c_4

$$y(x_2) = \big((1 + \Theta l_2)(\gamma y_1 + \delta y_2) + \Theta x_2 + 1\big)c_4 \tag{52}$$

$$\bar{y}(x_1) = \big((\varepsilon_3\Theta + \varepsilon_4)(\alpha\bar{y}_1 + \beta\bar{y}_2 + 1) + (\varepsilon_1\Theta + \varepsilon_2)x_1\big)c_4 \tag{53}$$

The buckling load can be obtained by satisfying equilibrium of shear force at axial load insertion point.

$$\frac{d}{dx_1}\left(\left(E_l + E_s\left(\frac{x_1}{l_1}\right)^n\right)\frac{d^2}{dx_1^2}\bar{y}(x_1)\right)\bigg|_{x_1=l_1} - \frac{d}{dx_2}\left(E_l + E_s\left(\frac{x_2}{l_2}\right)^n\frac{d^2}{dx_2^2}y(x_2)\right)\bigg|_{x_2=0} = 0 \tag{54}$$

The first real and positive roots of Eq. (49) are buckling loads of first modes. After replacing buckling load into Eq. (52), the normalized mode shape can be obtained.

4.2 Second method: Nontrivial solution

The problem includes eight homogeneous equations. A system of linear equations is homogeneous if all of the constant terms are zero. The solutions involving the number zero are considered trivial, while nonzero solutions are considered nontrivial. The deformation continuity and natural equations for calculating characteristic equation of beam with various end conditions are

$$\bar{y}|_{x_1=l_1} - y|_{x_2=0} = 0 \tag{55}$$

$$\bar{y}'|_{x_1=l_1} - y'|_{x_2=0} = 0 \tag{56}$$

$$(E_s + E_l)\bar{y}''|_{x_1=l_1} - E_l y''|_{x_2=0} = 0 \tag{57}$$

$$(E'\bar{y}'' + E\bar{y}''')|_{x_1=l_1} - (E'y'' + Ey''')|_{x_2=0} = 0 \tag{58}$$

Four boundary conditions at beam ends must be satisfied. The boundary condition of pinned end at right part of the beam is

$$y(x_2)|_{x_2=l_2} = 0 \tag{59}$$

$$\frac{d^2}{dx_2^2} y(x_2)\Big|_{x_2=l_2} = 0 \tag{60}$$

In the case of clamped support at right part of the beam, Eq. (61) is used instead of Eq. (60).

$$\frac{d}{dx_2} y(x_2)\Big|_{x_2=l_2} = 0 \tag{61}$$

Eq. (61) and Eq. (62) present the shear hinge boundary conditions at right part of the beam.

$$\frac{d}{dx_2}\left(\left(E_l + E_s\left(\frac{x_2}{l_2}\right)^n\right)\frac{d^2}{dx_2^2} y(x_2)\right)\Big|_{x_2=l_2} = 0 \tag{62}$$

The boundary condition of axial hinge at left part of the beam is

$$y(x_2)|_{x_2=l_2} = 0 \tag{63}$$

$$\frac{d^2}{dx_2^2} y(x_2)\Big|_{x_2=l_2} = 0 \tag{64}$$

The above mentioned equations are written in the matrix form.

$$\begin{bmatrix} \mathrm{m}_{11}(\mathrm{P}) & \dots & \mathrm{m}_{18}(\mathrm{P}) \\ \vdots & \ddots & \vdots \\ \mathrm{m}_{81}(\mathrm{P}) & \dots & \mathrm{m}_{88}(\mathrm{P}) \end{bmatrix}_{8\times 8} \begin{Bmatrix} \mathrm{c}_1 \\ \vdots \\ \mathrm{c}_8 \end{Bmatrix}_{8\times 1} = \begin{Bmatrix} 0 \\ \vdots \\ 0 \end{Bmatrix}_{8\times 1} \tag{65}$$

The arrays m_{ij} are obtained by considering derivatives of Eq_j (i.e., Eq. (55) to Eq. (58) and four boundary conditions at beam ends) with respect to the coefficients c_i.

$$\mathrm{m_{ij}} = \frac{\partial}{\partial c_i}\mathrm{Eq}_j \qquad\qquad i,j \in \{1,2,\dots,8\} \tag{66}$$

In the next step, the rows that include only one nonzero array and corresponding columns are deleted. The characteristic equation is calculated by vanishing determinant of the remained coefficient matrix.

$$\begin{vmatrix} \mathrm{m}_{11}(\mathrm{P}) & \dots & \mathrm{m}_{1(8-\mathrm{r})}(\mathrm{P}) \\ \vdots & \ddots & \vdots \\ \mathrm{m}_{(8-\mathrm{r})1}(\mathrm{P}) & \dots & \mathrm{m}_{(8-\mathrm{r})(8-\mathrm{r})}(\mathrm{P}) \end{vmatrix}_{(8-\mathrm{r})\times(8-\mathrm{r})} = 0 \tag{67}$$

The parameter r denotes number of removed rows or columns. The λ^{th} mode shape of buckled beam can be calculated as follows

$$\begin{Bmatrix} c_1 \\ \vdots \\ c_{7-r} \end{Bmatrix}_{(7-r)\times 1} = -c_{(8-r)(8-r)} \begin{bmatrix} m_{11}(P_\lambda) & \dots & m_{1(7-r)}(P_\lambda) \\ \vdots & \ddots & \vdots \\ m_{(7-r)1}(P_\lambda) & \dots & m_{(7-r)(7-r)}(P_\lambda) \end{bmatrix}^{-1}_{(7-r)\times(7-r)} \begin{Bmatrix} m_{1(8-r)}(P_\lambda) \\ \vdots \\ m_{(7-r)(8-r)}(P_\lambda) \end{Bmatrix}_{(7-r)\times 1} \quad (68)$$

in which P_λ is the λ^{th} positive root of characteristic equation ($P_\lambda \in \mathbb{R}$).

5. Result validation

The limit state is used to compare the results of current work with the well-known data in literature. To this purpose, the left part length, l_1 and linear material gradation, E_s of clamped-pinned beam are assumed to be negligible amounts with respect to the other parameters ($E_l = 2 \times 10^6\, kg/cm^2$, $E_s = 1 \times 10^2\, kg/cm^2$, $l_1 = 1mm$, $l_2 = 200cm$). The beam width and height are $10cm$ and $5cm$ respectively. The dimensionless critical load, $Pl_2^2/(\pi^2 E_l I)$ of pinned-clamped beam is obtained as 2.0438. The calculated dimensionless critical load is approached to the dimensionless critical load of homogeneous beam subjected to axial load at the pinned end (i.e. 2.0457). The results of current work for second and third modes (i.e., 6.0409 and 12.0353) are approached to the second and third dimensionless buckling loads of homogeneous beam (i.e. 6.0468 and 12.0471). In the case of clamped-clamped beam, the critical and second mode dimensionless buckling loads are calculated as 3.9961 and 8.1750. These results show a good agreement with the two first dimensionless buckling loads of homogeneous clamped-clamped beam (i.e., 4 and 8.1830). In the case of quadratic axially graded beam with clamped-pinned boundary conditions, the dimensionless critical load is calculated as 2.0437($m = 45$), which is approached to the critical load of pinned-clamped homogeneous beam subjected to constant axial load.

6. Results and discussions

Fig. 3 presents continues material gradation with linear and quadratic patterns in each part of the beam. In addition, the stepwise or discontinues material gradation through the longitudinal axis of the beam at parts junction or axial load insertion point is shown in Fig. (3). The diagram of thin beam characteristic equation for linear material gradation in axial direction with pinned-clamped (P-C) boundary conditions is depicted in Fig. 4. The mechanical and geometrical properties are assumed as $E_l = 2 \times 10^6\, kg/cm^2$, $E_s = 1 \times 10^6\, kg/cm^2$, $l_1 = 50cm$, $l_2 = 120cm$. The intersection points of diagram with the horizontal axis (characteristic equation roots) are buckling loads of first modes. The first three buckling loads are 230.5344 ton, 704.2887 ton and 1763.531 ton, respectively. The normalized mode shapes are illustrated in Fig. (5). The parameter l is $l_1 + l_2$.

The diagram of Euler-Bernoulli beam characteristic equation for linear pattern of material gradation in axial direction with axial hinge – shear hinge (AH-SHH) end conditions is shown in Fig. 6. The first three buckling loads are 86.099 ton, 332.700 ton and 860.401 ton, respectively. The normalized mode shapes of first three modes are illustrated in Fig. 7.

For conducting convergence analysis, the geometrical and mechanical properties are assumed as $E_l = 1.5E_s = 1.5 \times 10^6\, kg/cm^2$, $l_1 = l_2 = 100cm$ and $B = 2H = 10cm$. The prismatic

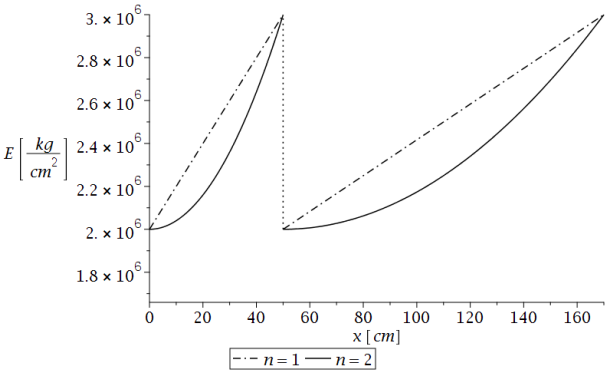

Fig. 3 The elasticity modulus variation in axial direction for various material gradation

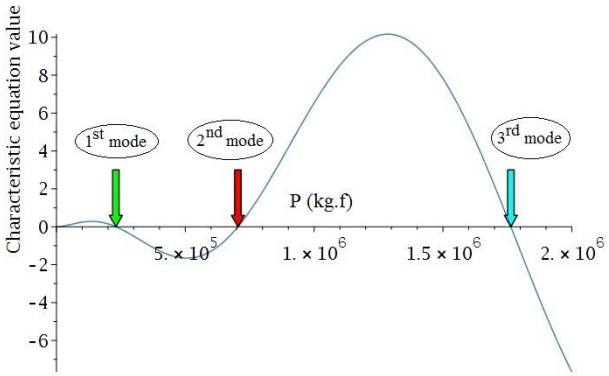

Fig. 4 Characteristic equation diagram for beam with pinned-clamped ends ($n = 1$)

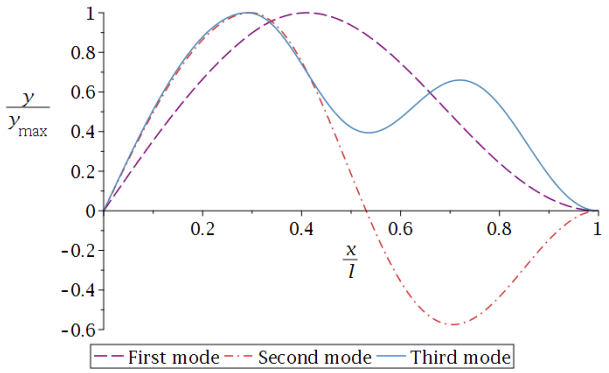

Fig. 5 Normalized deflection of axially graded beam with P-C ends (first three modes, $n = 1$)

beam is rested on axial hinge at left end and clamped restraint at right end (AH-C). The relative error reduction and convergence of solution for calculating critical load of axially graded Euler-Bernoulli beam with quadratic material gradation is illustrated in Fig. (8). The parameter m is truncation order of series in Eq. (18) - (19). By increasing truncation order the relative error is decreased. The critical loads of beam with discontinues quadratic gradation pattern in axial

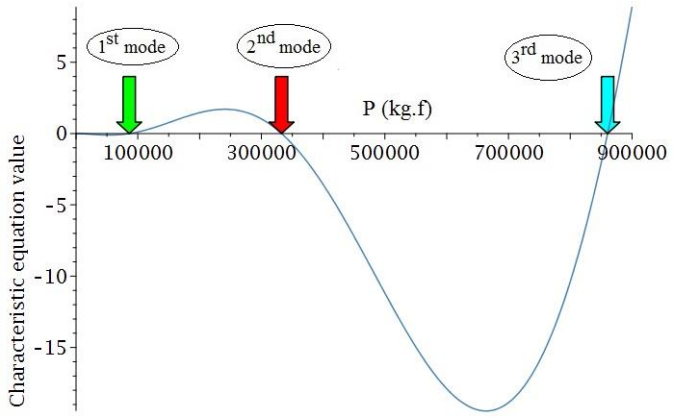

Fig. 6 Characteristic equation diagram for beam with AH-SHH ends ($n = 1$)

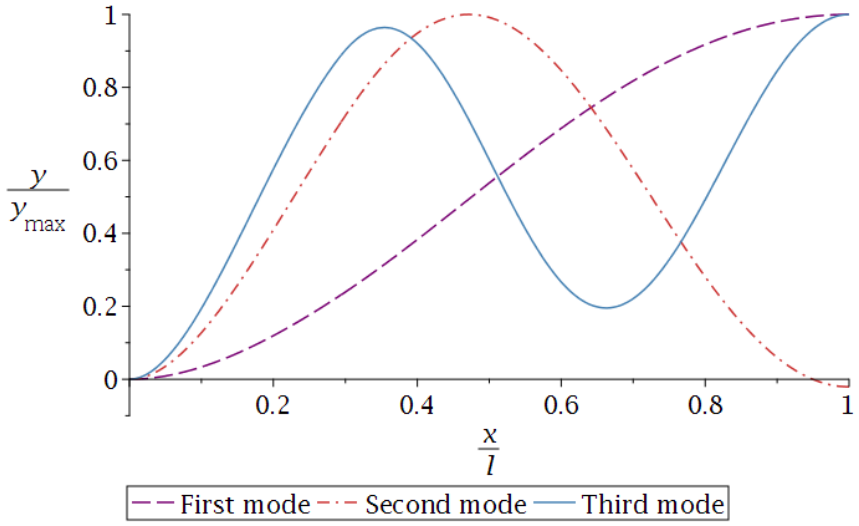

Fig. 7 Normalized deflection of axially graded beam with AH-SHH ends (first three modes, n=1)

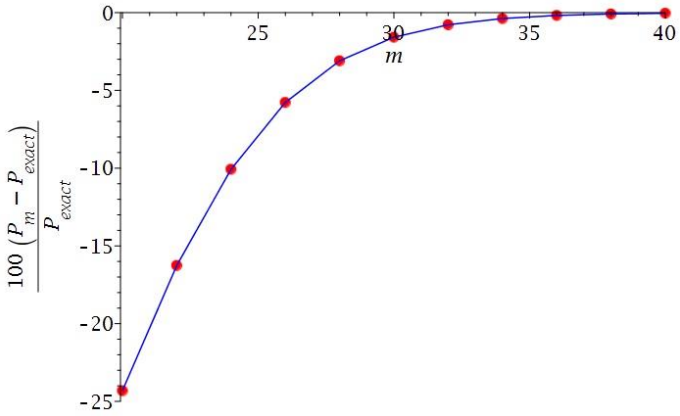

Fig. 8 Characteristic equation diagram for beam with AH-SHH ends ($n = 1$)

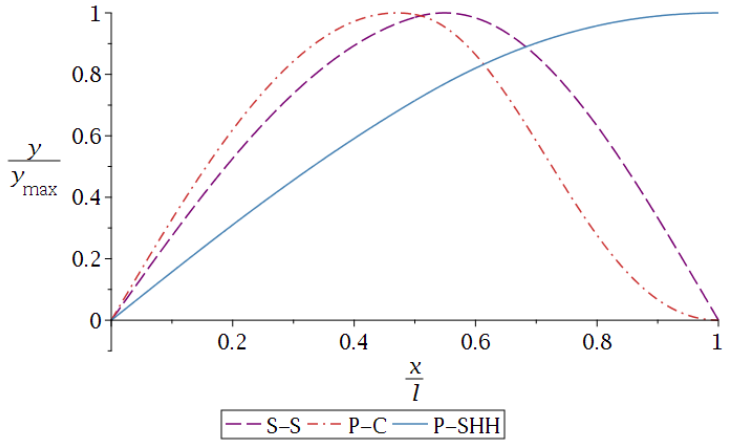

Fig. 9 Normalized deflection of axially graded beam with various boundary conditions ($n = 2$)

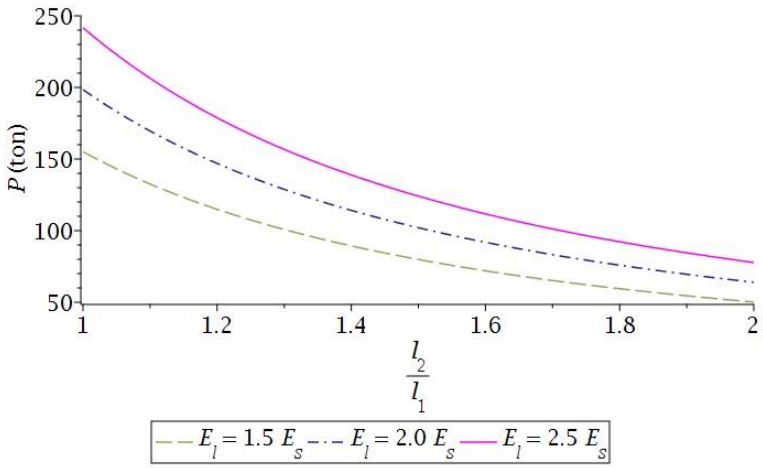

Fig. 10 Critical load of axially graded beam for various mechanical and geometrical properties (n=1,G=0)

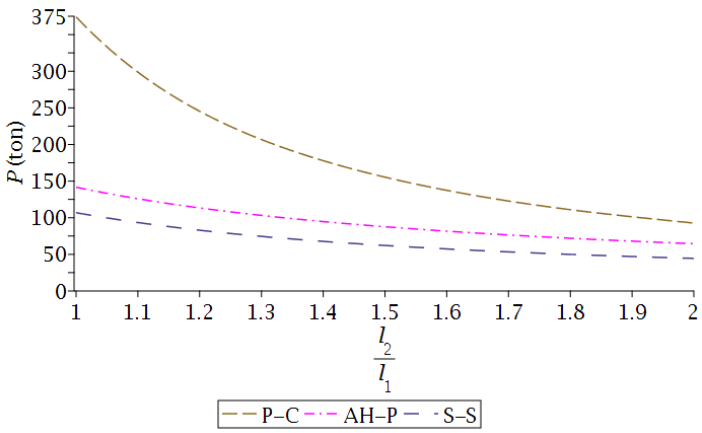

Fig. 11 Critical load of axially graded beam for various boundary conditions ($n = 2, G = 15\ ton$)

Table 1 Critical load for various mechanical and geometrical properties and axial gradation patterns in terms of ton

B.C.	E_1/E_s / l_2/l_1	1.5		2.0		2.5	
		$n=1$	$n=2$	$n=1$	$n=2$	$n=1$	$n=2$
S-S	1.0	155.10	70.305	198.47	91.899	241.67	113.44
	1.2	114.89	52.029	146.91	67.972	178.80	83.874
	1.4	89.346	40.422	114.17	52.782	138.88	65.109
	1.6	71.940	32.519	91.863	42.442	111.70	52.337
	1.8	59.457	26.855	75.874	35.033	92.224	43.187
	2.0	50.146	22.633	63.954	29.511	77.705	36.369
P-C	1.0	588.91	277.20	752.88	359.18	916.30	440.90
	1.2	380.11	178.26	484.33	230.33	588.11	282.19
	1.4	269.59	126.17	343.05	162.87	416.16	199.40
	1.6	203.03	94.880	258.16	122.42	313.03	149.84
	1.8	159.47	74.432	202.68	96.017	245.69	117.51
	2.0	129.22	60.250	164.20	77.717	198.99	95.104
AH-P	1.0	214.23	96.802	274.34	126.70	334.20	156.53
	1.2	166.92	75.291	213.34	98.392	259.57	121.43
	1.4	135.84	61.178	173.28	79.817	210.56	98.402
	1.6	113.92	51.237	145.03	66.734	176.01	82.183
	1.8	97.619	43.859	124.05	57.030	150.37	70.157
	2.0	85.016	38.162	107.85	49.544	130.58	60.886
AH-C	1.0	585.01	271.73	745.20	351.64	904.66	431.25
	1.2	410.86	190.49	523.01	246.44	634.64	302.17
	1.4	311.14	143.99	395.86	186.25	480.17	228.34
	1.6	247.77	114.44	315.03	147.99	381.95	181.41
	1.8	204.42	94.241	259.72	121.83	314.73	149.31
	2.0	173.11	79.666	219.75	102.94	266.15	126.12
P-SHH	1.0	31.188	14.250	39.030	18.162	46.827	22.067
	1.2	24.768	11.314	30.965	14.407	37.127	17.495
	1.4	20.266	9.2551	25.313	11.777	30.333	14.292
	1.6	16.955	7.7421	21.161	9.8447	25.343	11.941
	1.8	14.432	6.5897	17.999	8.3737	21.546	10.152
	2.0	12.457	5.6875	15.525	7.2228	18.577	8.7527
AH-SHH	1.0	91.686	41.876	115.34	53.701	138.85	65.468
	1.2	76.506	34.974	96.035	44.746	115.45	54.466
	1.4	65.185	29.832	81.678	38.090	98.075	46.303
	1.6	56.363	25.826	70.522	32.920	84.602	39.974
	1.8	49.277	22.609	61.587	28.779	73.829	34.913
	2.0	43.460	19.966	54.271	25.387	65.024	30.776

Table 2 Critical load of beam with shear force released at right end in terms of ton ($n = 2$)

B.C.	E_l/E_s / l_2/l_1	1.5		2.0		2.5	
		$n=1$	$n=2$	$n=1$	$n=2$	$n=1$	$n=2$
P-SHR	1.0	31.188	14.250	39.030	18.162	46.827	22.067
	1.2	24.768	11.314	30.965	14.407	37.127	17.495
	1.4	20.266	9.2551	25.313	11.777	30.333	14.292
	1.6	16.955	7.7421	21.161	9.8447	25.343	11.941
	1.8	14.432	6.5897	17.999	8.3737	21.546	10.152
	2.0	12.457	5.6875	15.525	7.2228	18.577	8.7527
AH-SHR	1.0	58.085	26.599	72.859	33.984	87.545	41.338
	1.2	47.658	21.835	59.623	27.821	71.517	33.780
	1.4	40.060	18.366	50.002	23.345	59.887	28.300
	1.6	34.263	15.723	42.684	19.943	51.057	24.141
	1.8	29.697	13.641	36.935	17.269	44.133	20.880
	2.0	26.012	11.961	32.307	15.118	38.569	18.259

direction with (S-S), (P-C) and (P-SHH) ends are 71.305, 278.20 and 15.250 ton, respectively ($G = 1\ \ ton$). The corresponding normalized mode shapes are illustrated in Fig. (9).

The critical load of simply supported (S-S) and axially graded beam with linear material gradation ($E_s = 10^6\, kg/cm^2$, $l_1 = 100cm$) for various ratios of elasticity modulus and various length ratios is presented in Fig. 10. The critical load is increased by increasing dimensionless ratio E_l/E_s and decreasing dimensionless ratio l_2/l_1. Fig. 11 demonstrates the critical load of beam with noncontinuous quadratic material gradation in axial direction and rested on shear layer ($G = 15\ \ ton$) for various boundary conditions and different length ratios ($E_l/E_s = 2$). In Figure (11), the critical load of beam with pinned-clamped (P-C) boundary conditions and critical load of beam with simply supported (S-S) end conditions are maximum and minimum loads, respectively.

The critical loads of thin beam ($\mathrm{E_s} = 10^6\,\mathrm{kg/cm^2}$, $\mathrm{L_1} = 100\mathrm{cm}, \mathrm{m} = 55$) for various mechanical and geometrical properties and axial gradation patterns are calculated and presented in Table 1. Also, critical loads of axially graded beam with shear force released at right end are reported in Table 2. The deflection and shear force are assumed to be zero at shear force released end.

7. Conclusions

For the first time, the buckling analysis of Euler-Bernoulli beam by considering stepwise material gradation in axial direction with linear and quadratic patterns rested on shear layer and subjected to piecewise compressive axial span-load function is conducted. The various boundary conditions including simply supported (S-S), pinned – clamped (P-C), axial hinge – pinned (AH-P), axial hinge – clamped (AH-C), pinned – shear hinge (P-SHH) and axial hinge – shear hinge (AH-SHH) as well as shear force released natural conditions are considered. The total potential energy is minimized by using variational calculus and the equilibrium differential equation is

derived. Two methods based on stepwise solution and nontrivial solution is proposed to obtain characteristic equation. The natural equations, deformation continuity as well as boundary conditions are written in the matrix form. The first buckling loads and corresponding mode shapes are calculated by employing matrix operations. The numerical results for various geometrical and mechanical properties, material gradation patterns, natural and boundary conditions are calculated and reported. The validity of the results is proved by obtaining similar results from two different methods. Moreover, in the limit state, the result validity is proved by observing a good agreement between results of current work and well-known data in literature. The convergence of the solution and relative error reduction are observed by increasing truncation order of the bases. Fast convergence and good compatibility with various end conditions are advantages of the proposed method based on nontrivial solution and matrix operations. It is observed that in each mode, the buckling load of beam with linear material gradation in axial direction is more than buckling load of quadratic axially graded beam with the same dimensions, boundary conditions and loading.

References

Alavi, S.H. and Eipakchi, H. (2020), "On the asymmetric transient responses of annular/circular viscoelastic plates based on shear deformation theory: an analytical approach", *Ships Offshore Struct*., **15**(2), 110-122. https://doi.org/10.1080/17445302.2019.1589048.

Arefi, M., Mohammad-Rezaei Bidgoli, E. and Rabczuk, T. (2019), "Thermo-mechanical buckling behavior of FG GNP reinforced micro plate based on MSGT", *Thin-Walled Struct*., **142**, 444-459. https://doi.org/10.1016/j.tws.2019.04.054.

Chen, J.S. and Wen, Z.S. (2019), "Deformation and vibration of a buckled beam constrained by springy walls", *Europee J. Mech. A/Solids*, **77**, 103791. https://doi.org/10.1016/j.euromechsol.2019.05.006.

Chengyi, C., Genshu, T. and Lei, Z. (2020), In-plane nonlinear buckling analysis of circular arches considering shear deformation. *Journal of Constructional Steel Research*, *164*, 105762. doi:https://doi.org/10.1016/j.jcsr.2019.105762.

Dai, T., Yang, Y., Dai, H.L., Tang, H. and Lin, Z.Y. (2019), "Hygrothermal mechanical behaviors of a porous FG-CRC annular plate with variable thickness considering aggregation of CNTs", *Compos. Struct*., **215**(1), 198-213. https://doi.org/10.1016/j.compstruct.2019.02.061.

Deng, J., Wang, X., Yuan, Z. and Zhou, G. (2019), "An efficient technique for simultaneous local and overall buckling analysis of stiffened panels", *Advan. Eng. Software*, **131**, 36-47. https://doi.org/10.1016/j.advengsoft.2019.03.002.

El-Galy, I.M., Saleh, B.I. and Ahmed, M.H. (2019), "Functionally graded materials classifications and development trends from industrial point of view", *SN Appl. Sci*., **1**(11). https://doi.org/10.1007/s42452-019-1413-4.

Falope, F.O., Lanzoni, L. and Radi, E. (2019), "Buckling of a Timoshenko beam bonded to an elastic half-plane: Effects of sharp and smooth beam edges", *Int. J. Solids Struct*., https://doi.org/10.1016/j.ijsolstr.2019.08.034.

Fang, J., Gu, J. and Wang, H. (2018), "Size-dependent three-dimensional free vibration of rotating functionally graded microbeams based on a modified couple stress theory", *Int. J. Mech. Sci*., **136**, 188-199. https://doi.org/10.1016/j.ijmecsci.2017.12.028.

Heydari, A. (2009), "Elasto-plastic analysis of thick walled fg tanks subjected to the internal pressure", *Int. J. Advan. Des. Manufact. Technol*., **3**(1), 11-18.

Heydari, A. (2011), "Buckling of functionally graded beams with rectangular and annular sections subjected to axial compression", *Int. J. Advan. Des. Manufact. Technol*., **5**(1), 25-31.

Heydari, A. (2013), "Analytical solutions for buckling of functionally graded circular plates under uniform radial compression using bessel function", *Int. J. Advan. Des. Manufact. Technol*., **6**(4), 41-47.

Heydari, A. (2015), "Spreading of plastic zones in functionally graded spherical tanks subjected to internal pressure and temperature gradient combinations", *Iran. J. Mech. Eng. Transactions ISME*, **16**(2), 5-25.
Heydari, A. (2018a), "Buckling analysis of tapered BDFGM nano-beam under variable axial compression resting on elastic medium", *Struct. Eng. Mech.*, **66**(6), 737-748. https://doi.org/10.12989/sem.2018.66.6.737.
Heydari, A. (2018b), "Exact vibration and buckling analyses of arbitrary gradation of nano-higher order rectangular beam", *Steel Composite Struct.*, **28**(5), 589-606. doi:https://doi.org/10.12989/scs.2018.28.5.589.
Heydari, A. (2018c), "Size-dependent damped vibration and buckling analyses of bidirectional functionally graded solid circular nano-plate with arbitrary thickness variation", *Struct. Eng. Mech.*, **68**(2), 171-182. https://doi.org/10.12989/sem.2018.68.2.171.
Heydari, A. (2019), "Elasto-plastic analysis of cylindrical vessel with arbitrary material gradation subjected to thermo-mechanical loading via DTM", *Arab. J. Sci. Eng.*, **44**(10), 8875-8891. https://doi.org/10.1007/s13369-019-03910-x.
Heydari, A. and Jalali, A. (2017), "A new scheme for buckling analysis of bidirectional functionally graded Euler beam having arbitrary thickness variation rested on Hetenyi elastic foundation", *Modares Mech. Eng.*, **17**(1), 47-55.
Heydari, A., Jalali, A. and Nemati, A. (2017), "Buckling analysis of circular functionally graded plate under uniform radial compression including shear deformation with linear and quadratic thickness variation on the Pasternak elastic foundation", *Appl. Math. Modelling*, **41**, 494-507. https://doi.org/10.1016/j.apm.2016.09.012.
Hu, Y., Khezri, M. and Rasmussen, K.J.R. (2019), "Analytical buckling solutions for Levy-type plates with edge and interior point-support(s)", *Thin-Walled Struct.*, **145**, 106419. https://doi.org/10.1016/j.tws.2019.106419.
Ismail, M., Shariati, M., Awal, A., Chiong, C., Chahnasir, E., Porbar, A. and Khorami, M. (2018), "Strengthening of bolted shear joints in industrialized ferrocement construction", *Steel Composite Struct.*, **28**(6), 681-690. https://doi.org/10.12989/scs.2018.28.6.681.
Kang, Z.T., Wang, Z.Y., Zhou, B. and Xue, S.F. (2019), "Galerkin weighted residual method for axially functionally graded shape memory alloy beams", *J. Mech.*, 1-15. https://doi.org/10.1017/jmech.2019.48.
Kharghani, N. and Soares, C.G. (2020), "Experimental, numerical and analytical study of buckling of rectangular composite laminates", *Europe. J. Mech. A/Solids*, **79**, 103869. https://doi.org/10.1016/j.euromechsol.2019.103869.
Lal, R. and Saini, R. (2019a), "On radially symmetric vibrations of functionally graded non-uniform circular plate including non-linear temperature rise", *Europe. J. Mech. A/Solids*, **77**, 103796. https://doi.org/10.1016/j.euromechsol.2019.103796.
Lal, R. and Saini, R. (2019b), "Thermal effect on radially symmetric vibrations of temperature-dependent FGM circular plates with nonlinear thickness variation", *Mater. Res. Express*, **6**(8), 0865f0861.
Lal, R. and Saini, R. (2019c), "Vibration analysis of functionally graded circular plates of variable thickness under thermal environment by generalized differential quadrature method", *J. Vib. Control*, **26**(1-2), 73-87. https://doi.org/10.1177%2F1077546319876389.
Lee, J.K. and Lee, B.K. (2019), "Free vibration and buckling of tapered columns made of axially functionally graded materials", *Appl. Math. Modelling*, **75**, 73-87. https://doi.org/10.1016/j.apm.2019.05.010.
Li, C., Shen, H.S. and Wang, H. (2019), "Thermal post-buckling of sandwich beams with functionally graded negative Poisson's ratio honeycomb core", *Int. J. Mech. Sci.*, **152**, 289-297. https://doi.org/10.1016/j.ijmecsci.2019.01.002.
Li, L., Li, X. and Hu, Y. (2018), "Nonlinear bending of a two-dimensionally functionally graded beam", *Compos. Struct.*, **184**, 1049-1061. https://doi.org/10.1016/j.compstruct.2017.10.087.
Li, L., Liao, W.H., Zhang, D. and Zhang, Y. (2019), "Vibration control and analysis of a rotating flexible FGM beam with a lumped mass in temperature field", *Composite Struct.*, **208**, 244-260. https://doi.org/10.1016/j.compstruct.2018.09.070.

Li, X., Li, L., Hu, Y., Ding, Z. and Deng, W. (2017), "Bending, buckling and vibration of axially functionally graded beams based on nonlocal strain gradient theory", *Compos. Struct.*, **165**, 250-265. https://doi.org/10.1016/j.compstruct.2017.01.032.

Magnucka-Blandzi, E., Wiśniewska-Mleczko, K. and Smyczyński, M.J. (2018), "Buckling of symmetrical circular sandwich plates with variable mechanical properties of the core in the radial direction", *Compos. Struct.*, **204**, 88-94. https://doi.org/10.1016/j.compstruct.2018.07.020.

Mittelstedt, S. and Mittelstedt, C. (2019), "Mixed-mode buckling of shear-deformable composite laminated I-beams", *Int. J. Mech. Sci.*, 105332. https://doi.org/10.1016/j.ijmecsci.2019.105332.

Rajasekaran, S. and Khaniki, H.B. (2019), "Bi-directional functionally graded thin-walled non-prismatic Euler beams of generic open/closed cross section Part I: Theoretical formulations", *Thin-Walled Struct.*, **141**, 627-645. https://doi.org/10.1016/j.tws.2019.02.006.

She, G.L., Ren, Y.R. and Yan, K.M. (2019), "On snap-buckling of porous FG curved nanobeams", *Acta Astronautica*, **161**, 475-484. https://doi.org/10.1016/j.actaastro.2019.04.010.

She, G.L., Ren, Y.R., Yuan, F.G. and Xiao, W.S. (2018), "On vibrations of porous nanotubes", *Int. J. Eng. Sci.*, **125**, 23-35. https://doi.org/10.1016/j.ijengsci.2017.12.009.

She, G.L., Shu, X. and Ren, Y.R. (2017), "Thermal buckling and postbuckling analysis of piezoelectric FGM beams based on high-order shear deformation theory", *J. Thermal Stresses*, **40**(6), 783-797. https://doi.org/10.1080/01495739.2016.1261009.

She, G.L., Yan, K.M., Zhang, Y.L., Liu, H.B. and Ren, Y.R. (2018, "Wave propagation of functionally graded porous nanobeams based on non-local strain gradient theory", *Europe. Phys. J. Plus*, **133**(9), 368. https://doi.org/10.1140/epjp/i2018-12196-5.

She, G.L., Yuan, F.G. and Ren, Y.R. (2017a), "Nonlinear analysis of bending, thermal buckling and post-buckling for functionally graded tubes by using a refined beam theory", *Compos. Struct.*, **165**, 74-82. https://doi.org/10.1016/j.compstruct.2017.01.013.

She, G.L., Yuan, F.G. and Ren, Y.R. (2017b), "Research on nonlinear bending behaviors of FGM infinite cylindrical shallow shells resting on elastic foundations in thermal environments", *Composite Struct.*, **170**, 111-121. https://doi.org/10.1016/j.compstruct.2017.03.010.

She, G.L., Yuan, F.G. and Ren, Y.R. (2017c), "Thermal buckling and post-buckling analysis of functionally graded beams based on a general higher-order shear deformation theory", *Appl. Math. Modelling*, **47**, 340-357. https://doi.org/10.1016/j.apm.2017.03.014.

She, G.L., Yuan, F.G. and Ren, Y.R. (2018), "On wave propagation of porous nanotubes", *Int. J. Eng. Sci.*, **130**, 62-74. https://doi.org/10.1016/j.ijengsci.2018.05.002.

She, G.L., Yuan, F.G., Karami, B., Ren, Y.R. and Xiao, W.S. (2019), "On nonlinear bending behavior of FG porous curved nanotubes", *Int. J. Eng. Sci.*, **135**, 58-74. https://doi.org/10.1016/j.ijengsci.2018.11.005.

She, G.L., Yuan, F.G., Ren, Y.R. and Xiao, W.S. (2017), "On buckling and postbuckling behavior of nanotubes", *Int. J. Eng. Sci.*, **121**, 130-142. https://doi.org/10.1016/j.ijengsci.2017.09.005.

She, G.L., Yuan, F.G., Ren, Y.R., Liu, H.B. and Xiao, W.S. (2018), "Nonlinear bending and vibration analysis of functionally graded porous tubes via a nonlocal strain gradient theory", *Composite Struct.*, **203**, 614-623. https://doi.org/10.1016/j.compstruct.2018.07.063.

Sobhy, M. and Zenkour, A.M. (2019), "Porosity and inhomogeneity effects on the buckling and vibration of double-FGM nanoplates via a quasi-3D refined theory", *Composite Struct.*, **220**, 289-303. https://doi.org/10.1016/j.compstruct.2019.03.096.

Toghroli, A., Darvishmoghaddam, E., Yousef Zandi, M.P., Safa, M., Abdullahi, M.A.M., Heydari, A., Khorami, M. (2018), "Evaluation of the parameters affecting the Schmidt rebound hammer reading using ANFIS method", *Comput. Concrete*, **21**(5). https://doi.org/10.12989/cac.2018.21.5.525.

Xiao, B.J. and Li, X.F. (2019), "Exact solution of buckling load of axially exponentially graded columns and its approximation", *Mech. Res. Communications*, **101**, 103414. https://doi.org/10.1016/j.mechrescom.2019.103414.

Yang, Y., Zhang, Y., Chen, W. and Yang, B. (2018), "On asymmetric bending of functionally graded solid circular plates", *Appl. Math. Mech.*, **39**(6), 767-782. https://doi.org/10.1007/s10483-018-2337-7.

Zhang, J., Chen, L. and Lv, Y. (2019), "Elastoplastic thermal buckling of functionally graded material beams", *Compos. Struct.*, **224**, 111014. https://doi.org/10.1016/j.compstruct.2019.111014.

CC